Scalable Autonomous Drone Flight in the Forest with Visual-Inertial SLAM and Dense Submaps Built without LiDAR

Sebastián Barbas Laina[1,3], Simon Boche[1], Sotiris Papatheodorou[1,2,3],
Dimos Tzoumanikas[2], Simon Schaefer[1], Hanzhi Chen[1] and Stefan Leutenegger[1,2,3]

Abstract— **Forestry constitutes a key element for a sustainable future, while it is supremely challenging to introduce digital processes to improve efficiency. The main limitation is the difficulty of obtaining accurate maps at high temporal and spatial resolution as a basis for informed forestry decision-making, due to the vast area forests extend over and the sheer number of trees. To address this challenge, we present an autonomous Micro Aerial Vehicle (MAV) system which purely relies on cost-effective and light-weight passive visual and inertial sensors to perform under-canopy autonomous navigation. We leverage visual-inertial simultaneous localization and mapping (VI-SLAM) for accurate MAV state estimates and couple it with a volumetric occupancy submapping system to achieve a scalable mapping framework which can be directly used for path planning. As opposed to a monolithic map, submaps inherently deal with inevitable drift and corrections from VI-SLAM, since they move with pose estimates as they are updated. To ensure the safety of the MAV during navigation, we also propose a novel reference trajectory anchoring scheme that moves and deforms the reference trajectory the MAV is tracking upon state updates from the VI-SLAM system in a consistent way, even upon large changes in state estimates due to loop-closures. We thoroughly validate our system in both real and simulated forest environments with high tree densities in excess of 400 trees per hectare and at speeds up to 3 m/s – while not encountering a single collision or system failure. To the best of our knowledge this is the first system which achieves this level of performance in such unstructured environment using low-cost passive visual sensors and fully on-board computation including VI-SLAM.**

I. INTRODUCTION

With 31% of Earth covered by forests or woodlands, their well-being is essential for all the inhabitants on Earth due to their essential task of reducing the carbon dioxide in the environment to produce oxygen. To move towards more sustainable, well-informed forest management, accurate and large-scale under-canopy tree-level data is required for more precise and data oriented decision-making. This challenging objective can only be achieved by leveraging the recent advances in robotics, environment perception and data analysis.

[1]Smart Robotics Lab, School of Computation, Information and Technology, Technical University of Munich. E-mail addresses: {sebastian.barbas, simon.boche, sotiris.papatheodorou, simon.k.schaefer, hanzhi.chen, stefan.leutenegger}@tum.de

[2]Smart Robotics Lab, Department of Computing, Imperial College London. E-mail addresses: {s.papatheodorou18, dimosthenis.tzoumanikas14, s.leutenegger}@ic.ac.uk

[3]Munich Institute of Robotics and Machine Intelligence (MIRMI).
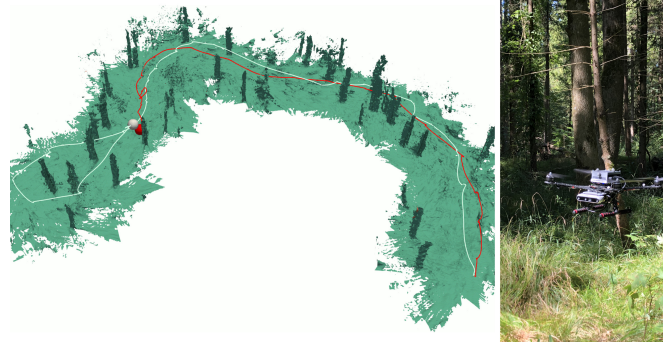
Fig. 1: Mesh of a real-world environment generated using our proposed approach. The executed mission consists of a back and forth trajectory with a small loop at the end. The red line shows the drone trajectory flying out, and the white one is the returning trajectory. The red sphere represents the start of the mission and the white one the end of it. Right: the drone used in these real-world experiments.

For precise data acquisition, aerial robots prove to be an ideal solution as they are not affected by the heterogeneous ground conditions present in a forest; and furthermore they are able to acquire data from all perspectives due to their available degrees of freedom. Nonetheless, forests present vast challenges: they must to a large extent be considered GPS denied environments when performing under-canopy missions; and these environments are cluttered and unstructured, demanding precise mapping and perhaps even consideration of moving branches for safe autonomous navigation.

To fly mapping missions autonomously, aerial vehicles require robust capabilities of state estimation, dense mapping and a flight controller which can track the commanded paths – in order to safely navigate the environment without collisions. At the same time, during mission, odometry drifts are unavoidable, but these need to be corrected continuously and especially upon loop closure to keep a consistent map representation for effective navigation therein and to communicate it to end-users.

State-of-the-art autonomous drone flying in forests typically relies on LiDAR, e.g. [1], [2] for precise and far-reaching range measurements. In this work, we aim to overcome such constraints employing only passive vision and an Inertial Measurement Unit (IMU), in a quest towards potentially cheaper, lighter, and thus more scalable drone systems which are flexibly deployable in cluttered environments

such as forests; able to pass through small gaps; and ideally without sacrificing flight velocity and endurance.

In short, the main contributions of this paper are:

- We present an autonomous drone system which performs under-canopy autonomous navigation with only (passive) visual and inertial sensors. It performs visual-inertial SLAM (VI-SLAM), deep-learning-based depth estimation from its stereo camera driving volumetric occupancy mapping in submaps, path planning and trajectory tracking – with all computations on-board.
- We introduce a novel approach to trajectory deformation at odometry rate, to continue performing trajectory tracking upon state estimation updates, most pronounced when loop-closures occur. This allows to seamlessly track planned paths without needing to stop upon odometry shifts.
- We demonstrate our approach in simulated and real-world forest environments of up to 467 trees per hectare and achieve flight velocities of up to 3 m/s without any collisions at all. To the best of our knowledge, we believe our system to be the first of its kind, i.e. not using LiDAR and flying in such dense forests while performing SLAM and mapping in the loop, allowing for missions which require precise mapping.
- We perform a mapping completeness and accuracy analysis to demonstrate the benefits of online maps generated via SLAM poses instead of visual inertial odometry. We demonstrate that with more loop-closures, the environment reconstruction quality is improved.

II. RELATED WORK

In this section we will focus on providing a comprehensive overview of complete frameworks for autonomous navigation, regardless of the specific sensors employed. Our goal is to create a vision-based system for autonomous navigation of MAVs that can operate in large, unstructured and cluttered environments, while building a map of the environment, for downstream tasks, and flying as fast as possible. Additionally, in large-scale autonomous navigation, a consistent communication network cannot be assumed, so a core capability of our system is that the algorithm must run on the MAV's onboard computer.

Several systems which leverage vision sensors for autonomous navigation have been proposed in the literature. One of the earliest versions of vision based navigation was presented in [3]. Based on a monocular camera and IMU sensors, the system was capable of performing state-estimation used for trajectory tracking. Simultaneously, data was streamed via WiFi to an off-board laptop which performed a 3D dense reconstruction of the environment via Multi-View stereo techniques. This method highlighted the potential of autonomous navigation based on vision systems but with certain limitations. The system relies on WiFi for the dense 3D reconstruction. In addition, there was no feedback between the perceived 3D reconstructed environment and the system, trajectories were given by an operator without any

collision avoidance mechanism onboard, leading to potentially risky missions.

Lin *et al.* present a seminal work in the area of vision-based autonomous navigation in [4]. The system leverages visual-inertial sensors to compute MAV odometry. The key distinction with our approach is their usage of monolithic 3D maps based on OctoMap[5], which is suboptimal for outdoor autonomous navigation for several reasons. Primarily the need to allocate a larger octree as the mission area increases, leading to slower data allocation of the octree. Secondly, the requirement to predefine the area of exploration poses a constraint. Moreover, as the odometry drift accumulates during the navigation, repeated geometric structures will appear within the map. The lack of a corrective mechanism for this issue can lead to an artificially more cluttered map hindering its use for path planning.

A system closely aligned with our work is [6], where an MAV based on visual-inertial sensors is capable of doing autonomous navigation while generating dense maps for path planning. While [6] relies on monolithic maps based on [7] and [8], we present a submapping approach based on [9], which can account for free, occupied and unknown space. The main differences between the systems are: [6] performs visual-inertial odometry (VIO) [10] while our proposed solution performs VI-SLAM and handles loop-closures, which is a challenge for autonomous systems; in [6] mapping is based on ESDFs, whilst our proposed system is based on occupancy values, allowing for faster depth integration to submaps; [6] performs both global and local planning, while our system relies on global planning; [6] relies on depth data from RGB-D sensors and our system leverages deep learning for stereo depth estimation; finally, the proposed system performs trajectory deformation to counteract odometry drift and loop-closure updates.

Another work which also relies on visual sensors for autonomous navigation in forestry environments was presented by Zhou *et al.* [11]. This work extends [12] by enabling swarms of MAVs to navigate in cluttered environments. Based on an ESDF mapping system, smooth trajectories are obtained to navigate around the present obstacles. The differences with our approach are: the use of VIO, based on [13], instead of SLAM; the system is designed to work with swarms of robots while our system is designed for only one; in [11], real world experiments were performed with a maximum navigation velocity of 1.5 m/s, lower than our maximum velocity of 3 m/s, a critical parameter for large scale missions.

A work which tackles the issue of high-speed navigation for MAVs in cluttered and unstructured environments is [14]. They propose an end-to-end learning approach based on privileged learning which allows the MAV to perform high-speed autonomous flights in environments outside the training set. Although their approach obtains higher velocities, it does not build a map of the environment, a component we consider crucial for downstream tasks and for collaborative robotics, as it serves for a common environment representation. The map of the environment also allows our approach to compute

collision-free reference trajectories whereas theirs assumes that a trajectory is provided, either by a higher-level planner or by the user. Also, this approach does not allow to perform missions which require a knowledge of mapping completeness or mapped area.

There are more works which rely on visual sensors for autonomous navigation [15], [16]. These rely on VIO, instead of SLAM, which is not able to correct for the state estimation drift which occurs over extended missions. As we will demonstrate, drift is the main source of error in map reconstruction, making drift correction techniques, such as loop-closure optimization, necessary for these types of applications. Accurate submaps and their poses are critical for safe navigation, as the accurate representations of free, occupied or unknown space are critical for safe path planning. Downstream tasks which require accurate online perception, such as exploration, where the goal is to completely explore a volume, also benefit from loop-closures and drift compensation.

Another prominent direction in autonomous navigation are systems which rely on LiDAR sensors. These systems have demonstrated an improved performance if compared with vision based systems due to the unpaired depth perception capabilities of these sensors. Some of the most important work regarding autonomous navigation with LiDAR sensors was presented in [2], who were the winners of the DARPA Subterranean Challenge. This team included MAVs to perform subterranean exploration in conjunction with legged robots. To perform state estimation, they relied in multi-sensor fusion of visual and thermal imagery, LiDAR depth data, inertial cues, and kinematic pose estimates based on [17]. This sensor redundancy provided robustness to sensor degradation or malfunctioning.

Another example of these systems was presented by Liu *et al.* [1]. This system loosely couples semantic LiDAR odometry and visual inertial states to estimate the odometry of the MAV. They base their work on [18], [19] and they improve SLOAM [20] by incorporating visual-inertial odometry and a lightweight semantic segmentation network designed for LiDAR data. They also showcase their system in under-canopy forest navigation and, to the best of our knowledge, it is the only system which leverages SLAM instead of plain odometry for state estimation. Being able to handle loop-closures, which produce odometry discontinuities, is a major issue for autonomous navigation with a SLAM framework. In their approach, they perform path planning in a visual odometry reference frame. On each update, the drift between the SLAM reference frame and the visual odometry reference frame is computed and the planned trajectory is transformed with this estimated drift. In our approach we anchor the trajectory on prior poses, as we know they were in free space. We then deform the trajectory based on the updates to these pose anchors. Thanks to the anchoring technique, we do not need to update in parallel a VIO and a SLAM system, but can work with a single state-estimator, reducing the overall computational cost of the system .

Compared with these systems, the main difference of the proposed method is that it does not rely on LiDAR sensors but only on passive visual sensors. This has two main advantages: it reduces the mass of the system, which reduces battery consumption, and it also reduces the cost of the system.

III. PROPOSED APPROACH

In this section we will present the different modules which build our system. A schematic overview is presented in Fig. 2

A. MAV platform

We use a custom-built quadrotor as depicted in Fig. 1 consisting of a HolybroS500 V2 ARF-Kit airframe[1], a PX4 flight controller[2], an Intel RealSense D455[3] (of which we only use the IR stereo images and the IMU), and an NVIDIA Jetson Orin NX (16GB)[4] for processing (CPU and GPU) that is carried out entirely on-board. The total mass including battery amounts to 1.3 kg, allowing flight times around 10 minutes. We also replicated the setup in simulation using Ignition Gazebo[5].

B. Notation and Definitions

The used VI-SLAM [21] tracks a moving body with a mounted IMU and several cameras relative to a static World coordinate frame $\underrightarrow{\mathcal{F}}_W$. The IMU coordinate frame is denoted as $\underrightarrow{\mathcal{F}}_S$ and the camera frames as $\underrightarrow{\mathcal{F}}_{C_i}$, whereby we use a stereo setup and therefore $i \in 1, 2$. Left-hand indices denote coordinate representation. Homogeneous position vectors (denoted in italic font) can be transformed with T_{AB}, meaning $_A r_P = T_{AB}\,_B r_P$.

C. State Estimation

Our state estimation module is based on the existing VI-SLAM system OKVIS2. We will provide a brief recap of the key components of this work. For more details of OKVIS2 please refer to [21]. OKVIS2 requires IMU measurements and stereo images as inputs to perform the state estimation and the sparse map of the environment which is based on the visual landmarks extracted from the images. The state representation in this work is:

$$\mathbf{x}_l = \left[_W\mathbf{r}_S^T, \mathbf{q}_{WS}^T, _W\mathbf{v}^T, \mathbf{b}_g^T, \mathbf{b}_a^T \right]^T, \tag{1}$$

i.e. the position $_W\mathbf{r}_S$ (of the IMU frame origin) expressed in World coordinates, its orientation quaternion $\mathbf{q}_{WS}$, velocity $_W\mathbf{v}$, and gyroscope and accelerometer biases $\mathbf{b}_g$ and $\mathbf{b}_a$, respectively. A new state $\mathbf{x}_l$ is estimated when a pair of stereo images is received. In the estimator, two non-linear least squares optimizations are present: one executed in a real-time manner, in which the optimization runs over the last T frames, M keyframes, considering IMU measurements in-between, as well as reprojection errors and pose-graph
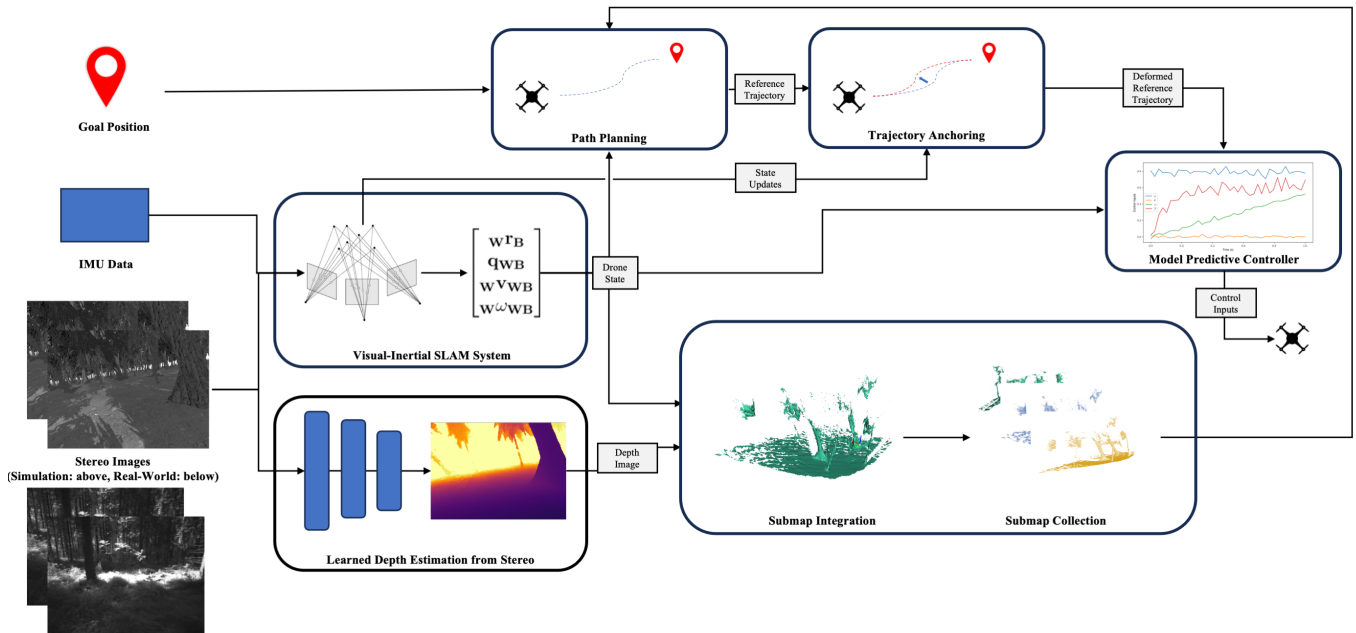
Fig. 2: Overall approach overview: incoming stereo frames and IMU measurements are consumed by the OKVIS2 VI-SLAM system. In parallel, the stereo images are processed by a CNN to output a depth map, which is then integrated into occupancy submaps. These in turn are used by a planner, generating a reference trajectory to be followed by the MPC. Upon state updates, especially pronounced after loop-closures, the trajectory is kept anchored to state estimates, i.e. moved and deformed in-line with the estimates and submaps.

errors formulated from marginalised co-observation; and a second optimization problem, using the exact same factor graph, is triggered on loop-closure in the background, which optimises older states around the loop, too. This means, when processing a new frame, not only its state $\mathbf{x}_l$ is estimated, but possibly many prior states $\mathbf{x}_{l-k}$ are also updated.

D. Model Predictive Controller

The (linear) model predictive control (MPC) is based on our prior work presented in [22], although modifications were done so it could accept the trajectory updates processed by the trajectory anchoring as described below in Sec. III-F. Previously, the system would receive the odometry states asynchronously from the trajectory states to be tracked. For a correct trajectory tracking under the presence of major odometry changes, as it happens with loop closures, the odometry update has to be processed synchronously with the deformed trajectory to ensure smooth and safe navigation.

The MPC obtains odometry updates at a minimum rate of 40Hz to compute the attitude control sent to the MAV's internal PX4 attitude controller via MAVROS[6]. To achieve a higher rate than the framerate, IMU integration is performed from the most recent state estimate to the most recent IMU measurement received.

E. Submap Interface

To perform tasks such as path planning and navigation, a mapping system needs to store the information of the

perceived environment as a basis of planning and executing actions. As the sparse pointclouds produced by OKVIS2 are not sufficient to this end, we adopt a dense mapping framework, based on supereight2 [9], an octree-based volumetric mapping approach which can represent occupied, free and unobserved space. At the same time, it leverages multi-resolution, enabling faster integration of depth or range measurements into each map, as well as faster collision checks during path planning.

To account for inaccuracies and drift corrections of the underlying SLAM system, it is quintessential to refrain from the concept of a monolithic volumetric map. Otherwise maps inconsistent with trajectory estimates are constructed, which are artificially cluttered with duplicated structure after corrections – in essence entirely useless for any form of safe navigation therein.

We therefore adopt a submapping approach, in which submaps are associated with keyframes from OKVIS2 and rigidly move with them. This is based on the assumption that locally, pose drift is negligible, allowing to fuse several depth images into a local submap.

As classical stereo-matching algorithms could fail in challenging outdoor scenarios and only yield sparse output, we developed a deep stereo network able to infer dense depth based on [23], and fine-tuned it with large-scale synthetic forestry data from [24]. To generate the map, given a set of depth images $\mathbf{D}_t$ obtained via depth stereo estimation at a time step t, we aim to generate an occupancy-based volumetric map. OKVIS2 computes a state $\mathbf{x}_t$ from the same
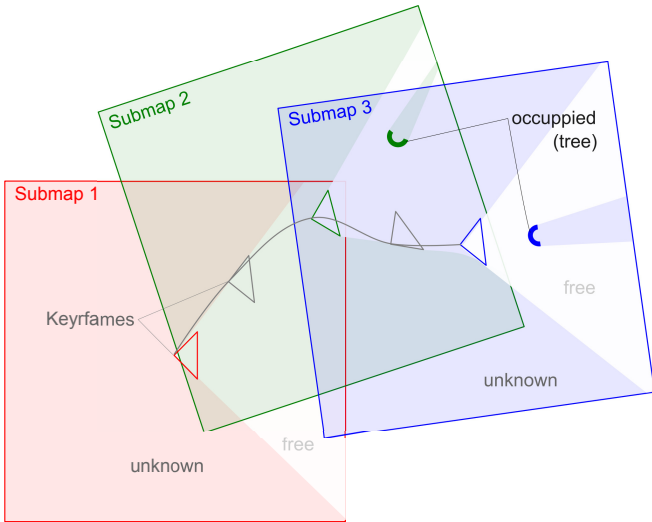
Fig. 3: Submap generation example every two OKVIS2 keyframes: note the differentiation between unknown, free, and occupied space per submap. Submaps are aligned with the respective keyframes and move with them when OKVIS2 re-estimates them – which is pronounced upon loop-closure.
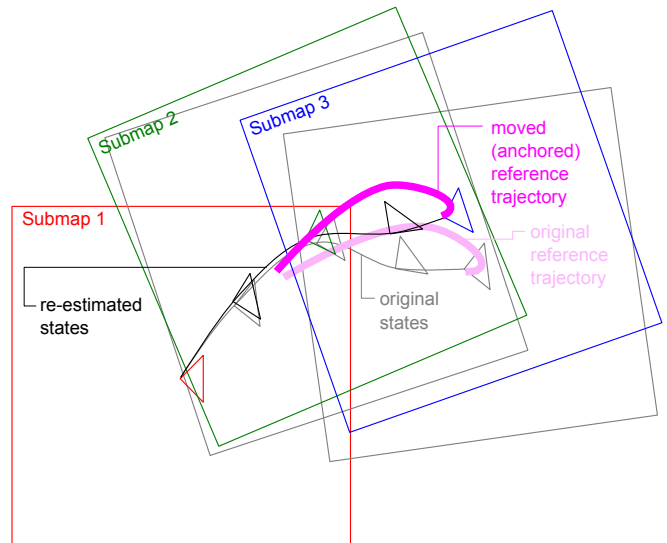

Fig. 4: Reference trajectory anchoring: when estimated states change, e.g. upon loop closure, the planned reference trajectory moves in-line with the states and submaps associated with some of the keyframe states. The previous state trajectory, keyframe, and submap poses are drawn in gray, whereas the updated state trajectory is black. The previous trajectory (light pink) is moved and deformed (pink) in line with the submaps (illustrative example with exaggerated change).

stereo images, thus $\mathbf{D}_t$ is inherently associated with the pose estimates in $\mathbf{x}_t$, thus we can directly use the pose of camera 1, in which $\mathbf{D}_t$ is expressed, i.e. $T_{WC_{1,t}} = T_{WS_t} T_{SC_1}$, where T_{SC_1} denotes the extrinsics calibration of camera 1.

The submap generation policy is based on the keyframe selection done by OKVIS2. Every n keyframes, a new submap, with pose T_{WS_k}, is generated, where the upcoming depth images will be integrated as they are processed, with the k-th keyframe of the trajectory. An example of the submap generation policy can be found in Fig. 3. As both T_{WS_k} and $T_{WC_{1,t}}$ are known, the relative transform $T_{S_k C_{1,t}}$ can be computed, i.e. the pose of the depth frame at time step t relative to the submap coordinate frame corresponding to the pose at time step k, $\underrightarrow{\mathscr{F}}_{S_k}$, allowing depth frame integration. On keyframe state updates, the poses of submaps move accordingly.

F. Path Planning and Reference Trajectory Anchoring

Our path planning is based on OMPL [25], specifically using the Informed RRT* [26] algorithm. To extend the path planner to the submap structure leveraged in our work, we assume that if a path segment (comprised of a cylinder and a half-sphere at the end of the segment, both of the same radius) is free in any of the last S submaps, it is a valid segment to navigate through. As our occupancy maps distinguish between free, occupied and unknown space, we will consider a segment free if the log-odds occupancy value is below a threshold $\alpha < 0$ which only occurs in free-space.

Once a safe path is returned, it is converted into a trajectory, by accounting for the maximum velocity $v_{\max}$ and acceleration $a_{\max}$ that we consider to decelerate and accelerate on sharp turns. This reference trajectory will undergo the process of what we call trajectory anchoring, effectively

moving the reference in-line with updates from the state estimator. "Jumps" in state estimates would otherwise lead to undesired erratic drone motion and ultimately to a crash, as the drone will aim to navigate to the previous trajectory state which represents a different environment location. Furthermore, we need to ensure that the planned reference trajectory remains both in free space after the submap poses are updated, as well as that it remains continuous, i.e. the change must not break apart the reference trajectory.

Our approach as visualized in Fig. 4 anchors each reference state to a set $\mathscr{S}$ of states $\mathbf{x}_s$, $s \in \{1, \ldots, S\}$ estimated by OKVIS2. The reference trajectory states will be updated as the anchor states $\mathbf{x}_s$ update their corresponding poses.

A reference trajectory contains references (superscript "ref") $\mathbf{x}_j^{\text{ref}} = ({}_W\mathbf{r}_{WS_j}^{\text{ref}}, \mathbf{q}_{WS_j}^{\text{ref}}, {}_W\mathbf{v}_j^{\text{ref}})$, with $j \in \{1, \ldots, J\}$ (and corresponding timestamps), which are anchored to the estimated OKVIS2 states in $\mathscr{S}$ via the algorithm of k-nearest neighbours, using the distance metric:

$$d_{j,s} = ||_W\mathbf{r}_{WS_j}^{\text{ref}} - {}_W\mathbf{r}_{S_s}||. \tag{2}$$

We associate every pair j,s with the relative transformation $T_{S_s S_j}$ and a weight $w_{j,s}$:

$$w_{j,s} = \frac{1/d_{j,s}}{\sum_{j=1}^{S} 1/d_{j,s}}. \tag{3}$$

Upon a state update, trajectory state positions are updated as follows:

$$_W\mathbf{r}_{WS_j}^{\text{ref'}} = \sum_{s=1}^{S} w_{j,s} T_{WS_s} {}_{S_s}\mathbf{r}_{S_j}, \tag{4}$$

where $\boldsymbol{T}_{WS_s}$ is the latest anchor pose as estimated by OKVIS2. The orientation $\mathbf{q}_{WS_j}^{\text{ref'}}$ is updated to the weighted average of $\mathbf{q}_{S_sS_j}, s \in \{1\dots S\}$ using the weights already computed as above by following the method from [27] . We also apply the respective orientation changes to the velocities.

IV. EVALUATION

To validate our method, we present two sets of experiments. The first one is done in simulation where quantitative results can be obtained for the estimator and the map quality. The second set of results is obtained from real-world experiments, where qualitative results are presented.

The parameters in both experiments were kept constant. The voxel resolution of the volumetric mapping was set to 10 cm, the planning time set to 0.5 s and the target maximum velocity was set to 3 m/s. The OKVIS2 hyperparameters were kept constant for both the simulator and the real-world experiments for a fair comparison, matching the computational resources of the Jetson Orin NX. In both cases, loop-closures were present, necessitating trajectory anchoring.

A. Simulation Experiments

Our simulator is based on the Ignition Gazebo simulation environment. In this simulation, we have created an artificial forest which contains 620 trees in a squared shaped surface area of 16'384 m^2, i.e. 378 trees per hectare. According to [28], Swiss forests come with an average tree density of 690 trees on the same surface area, validating the realism of our simulation. To add more realism to the simulation, we use PX4's simulation in the loop capabilities to interact with the drone, equivalently to the real world setup – including MAVROS for communication between the MPC and the PX4, instead of assuming perfect tracking.

In order to demonstrate the capability of our system to perform long missions in presence of loop closures, and the superior quality of maps generated by a system leveraging SLAM rather than just VIO, we evaluate on two mission types: the first using a classic lawnmower pattern reference path and the second a slight modification of the former which triggers more loop-closures by revisiting previously mapped areas. Both patterns result in large loop closures so as to validate the performance and safety of the system and particularly the trajectory anchoring module. A total of 12 missions were executed, *without a single MAV collision*. Trajectories following the lawnmower path had an average length of 1869.78 m while those following the modified version had an average length of 2363.64 m. An example of each mission type and the resulting trajectories is shown in Fig. 5 while an example of trajectory anchoring upon loop-closure is presented in Fig. 6.

Fig. 7 shows the velocity profile of a mission using the modified lawnmower pattern obtained from the ground-truth odometry provided by the simulator. The average velocity is approximately 1.3 m/s even though the target velocity is 3m/s. This is due to the large amount of aggressive maneuvers the MAV had to perform to navigate between
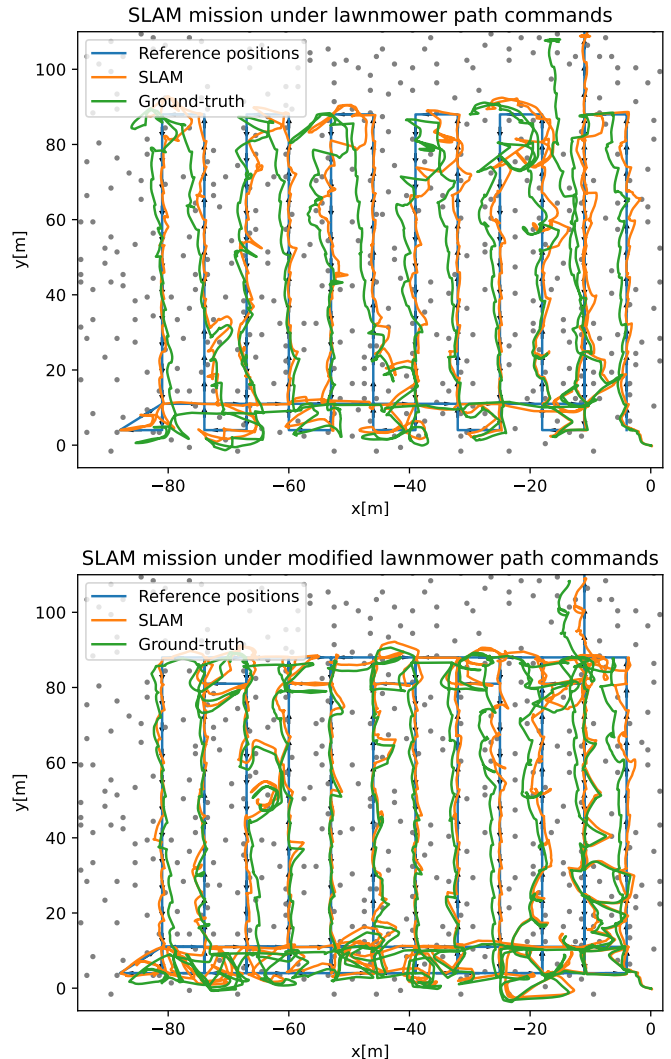

Fig. 5: Overhead views of two simulation experiments, one using a lawnmower pattern on the top and one using the proposed modified lawnmower pattern which triggers more loop-closures on the bottom. The images show the MAV reference positions, the live trajectory estimated by the OKVIS2 SLAM system and the corresponding ground-truth trajectory. Tree positions are shown as dots. The reference positions can't always be accurately tracked due to the presence of trees.

the trees, requiring a lower velocity. The target velocity was achieved on the longer and straighter segments.

To demonstrate the superior mapping quality obtained by leveraging SLAM for state estimation, we evaluate the accuracy and completeness of the mesh reconstructions obtained via SLAM and VIO. We also evaluate the reconstructions using the ground-truth poses and depth maps corresponding to the SLAM and VIO missions as a best-case-scenario. The final reconstruction is the combination of the submap meshes. Accuracy is computed as the root-mean-square error and completeness is computed as the percentage of the ground-truth mesh vertices for which there is a reconstructed
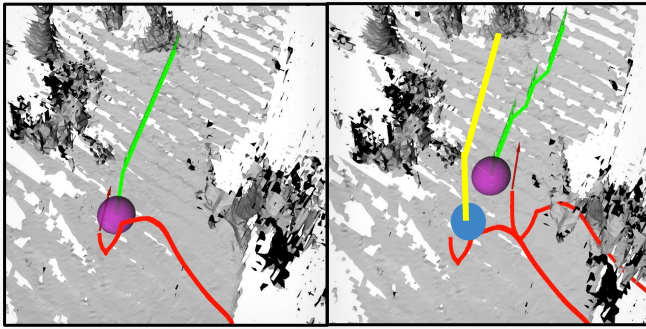
Fig. 6: Trajectory anchoring when performing a mission in the simulator. Left: MAV pose (red arrow), estimated past trajectory (red line), current MPC reference (violet sphere) and reference trajectory (green line) before a loop-closure was detected. Right: situation after the loop-closure with deformed estimates and anchored trajectory. The blue circle and the yellow line represent an estimate of the MPC reference and reference trajectory if trajectory anchoring were not operating – highlighting possible catastrophic failures if not handled.
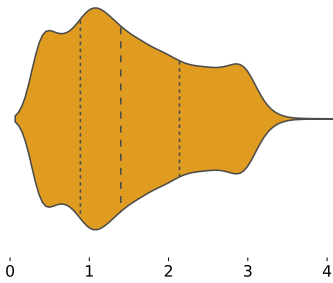

Fig. 7: MAV velocity distribution in m/s for a simulated mission with a reference velocity of 3 m/s and a trajectory length of 2363.58 m.

		Acc. (m)↓	Compl. (%)↑
SLAM	Lawnmower	0.280	69.62
VIO		0.240	48.71
GT SLAM		0.103	71.86
GT VIO		0.104	69.85
SLAM	Modified Lawnmower	0.190	71.34
VIO		0.230	28.08
GT SLAM		0.105	72.14
GT VIO		0.105	74.32

TABLE I: Mesh reconstruction accuracy and completeness for both mission types using SLAM and VIO as well as using ground-truth poses and depth images (GT SLAM/VIO rows).

mesh vertex within 50 cm.

The quantitative evaluation results are presented in Table I. The ground-truth mesh reconstructions do not achieve 100% completeness because there are regions of the environment that are unobservable from the followed trajectories, e.g. the higher parts of trees. It can be seen that the drift correction due to loop-closures improves both the reconstructed mesh quality and the trajectory accuracy in both mission types. The modified lawnmower pattern results in further improvement in mesh accuracy and completeness in the SLAM case due to the higher amount of loop closures triggered homogeneously throughout the mission.

B. Real World Experiments

For the real-world experiments, two people were required: a safety-pilot in case of unexpected malfunctioning and an operator. The latter would manually set the 3D pose where the drone should fly.The overall mission consisted of doing a path forward, then turn around and return in the opposite direction to prevent short loop-closures as shown in Fig. 1. During the return phase, the planned paths were longer, because prior submaps could be used for path planning. Near home, an extra detour was done to be able to change again the orientation and have the same start pose to finally trigger a long loop-closure. OKVIS2 processed stereo images at 15Hz and depth images were generated at 5Hz on average.

For these experiments we have roughly determined the position drift between the start and end positions to be less than 1 meter *before* loop-closure – since the drone was commanded back to the start. According to the OKVIS2 odometry, the total distance travelled during the mission was of 226.71m. Thus the estimator position drift amounts to $< 0.5\%$ of distance travelled, which is substantially more accurate than the numbers reported in [1] ($> 1.0\%$).

The maximum velocity achieved was a peak of 4 m/s according to OKVIS2 odometry, although the average velocity was at 1.2 m/s with the top and bottom quartiles being at 1.8 m/s and 0.6 m/s, respectively. *No collisions* occurred during the mission, and *no interventions* had to be made, as all planned segments were assessed to be safe, and in fact flown safely by the controller.

The approximate density of the forest in the area of the real-world experiments amounted to 467 trees per hectare, which is even denser than the simulated forest or a comparable forest area in Switzerland.

V. CONCLUSION

In this paper, we presented an MAV system which relies solely on passive visual sensors and an IMU to perform autonomous under-canopy navigation in forests. Onboard visual-inertial SLAM is in charge of MAV state estimation. We propose a volumetric occupancy submapping system to achieve a scalable mapping representation of the environment and reduce the reconstruction errors which arise in monolithic maps under drifting and brusquely changing state estimates. We also introduce an approach of trajectory anchoring to ensure safe navigation upon abrupt changes in odometry due to loop closures. To demonstrate the method, we validated the system both in simulation and in a real-world environment – demonstrating safe flight at up to 3 m/s without a single collision or unsafe planning instance.

REFERENCES

[1] X. Liu, G. V. Nardari, F. C. Ojeda, Y. Tao, A. Zhou, T. Donnelly, C. Qu, S. W. Chen, R. A. Romero, C. J. Taylor *et al.*, "Large-scale autonomous flight with real-time semantic SLAM under dense forest canopy," *IEEE Robotics and Automation Letters*, vol. 7, no. 2, pp. 5512–5519, 2022.

[2] M. Tranzatto, T. Miki, M. Dharmadhikari, L. Bernreiter, M. Kulkarni, F. Mascarich, O. Andersson, S. Khattak, M. Hutter, R. Siegwart *et al.*, "CERBERUS in the DARPA Subterranean Challenge," *Science Robotics*, vol. 7, no. 66, p. eabp9742, 2022.

[3] M. Faessler, F. Fontana, C. Forster, E. Mueggler, M. Pizzoli, and D. Scaramuzza, "Autonomous, vision-based flight and live dense 3D mapping with a quadrotor micro aerial vehicle," *Journal of Field Robotics*, vol. 33, no. 4, pp. 431–450, 2016.

[4] Y. Lin, F. Gao, T. Qin, W. Gao, T. Liu, W. Wu, Z. Yang, and S. Shen, "Autonomous aerial navigation using monocular visual-inertial fusion," *Journal of Field Robotics*, vol. 35, no. 1, pp. 23–51, 2018.

[5] A. Hornung, K. M. Wurm, M. Bennewitz, C. Stachniss, and W. Burgard, "OctoMap: An efficient probabilistic 3D mapping framework based on octrees," *Autonomous robots*, vol. 34, pp. 189–206, 2013.

[6] H. Oleynikova, C. Lanegger, Z. Taylor, M. Pantic, A. Millane, R. Siegwart, and J. Nieto, "An open-source system for vision-based micro-aerial vehicle mapping, planning, and flight in cluttered environments," *Journal of Field Robotics*, vol. 37, no. 4, pp. 642–666, 2020.

[7] H. Oleynikova, Z. Taylor, M. Fehr, R. Siegwart, and J. Nieto, "Voxblox: Incremental 3D Euclidean signed distance fields for on-board MAV planning," in *2017 IEEE/RSJ International Conference on Intelligent Robots and Systems (IROS)*, 2017, pp. 1366–1373.

[8] A. Millane, Z. Taylor, H. Oleynikova, J. Nieto, R. Siegwart, and C. Cadena, "C-blox: A scalable and consistent TSDF-based dense mapping approach," in *2018 IEEE/RSJ International Conference on Intelligent Robots and Systems (IROS)*, 2018.

[9] N. Funk, J. Tarrio, S. Papatheodorou, M. Popović, P. F. Alcantarilla, and S. Leutenegger, "Multi-resolution 3D mapping with explicit free space representation for fast and accurate mobile robot motion planning," *IEEE Robotics and Automation Letters*, vol. 6, no. 2, pp. 3553–3560, 2021.

[10] T. Schneider, M. Dymczyk, M. Fehr, K. Egger, S. Lynen, I. Gilitschenski, and R. Siegwart, "maplab: An open framework for research in visual-inertial mapping and localization," *IEEE Robotics and Automation Letters*, vol. 3, no. 3, pp. 1418–1425, 2018.

[11] X. Zhou, J. Zhu, H. Zhou, C. Xu, and F. Gao, "Ego-swarm: A fully autonomous and decentralized quadrotor swarm system in cluttered environments," in *2021 IEEE international conference on robotics and automation (ICRA)*. IEEE, 2021, pp. 4101–4107.

[12] X. Zhou, Z. Wang, H. Ye, C. Xu, and F. Gao, "Ego-planner: An ESDF-free gradient-based local planner for quadrotors," *IEEE Robotics and Automation Letters*, vol. 6, no. 2, pp. 478–485, 2020.

[13] H. Xu, L. Wang, Y. Zhang, K. Qiu, and S. Shen, "Decentralized visual-inertial-uwb fusion for relative state estimation of aerial swarm," in *2020 IEEE international conference on robotics and automation (ICRA)*. IEEE, 2020, pp. 8776–8782.

[14] A. Loquercio, E. Kaufmann, R. Ranftl, M. Müller, V. Koltun, and D. Scaramuzza, "Learning high-speed flight in the wild," *Science Robotics*, vol. 6, no. 59, p. eabg5810, 2021.

[15] T. Cieslewski, E. Kaufmann, and D. Scaramuzza, "Rapid exploration with multi-rotors: A frontier selection method for high speed flight," in *2017 IEEE/RSJ International Conference on Intelligent Robots and Systems (IROS)*, 2017, pp. 2135–2142.

[16] Z. Zhang and D. Scaramuzza, "Perception-aware receding horizon navigation for MAVs," in *2018 IEEE International Conference on Robotics and Automation (ICRA)*, 2018, pp. 2534–2541.

[17] S. Khattak, H. Nguyen, F. Mascarich, T. Dang, and K. Alexis, "Complementary multi–modal sensor fusion for resilient robot pose estimation in subterranean environments," in *2020 International Conference on Unmanned Aircraft Systems (ICUAS)*. IEEE, 2020, pp. 1024–1029.

[18] K. Mohta, K. Sun, S. Liu, M. Watterson, B. Pfrommer, J. Svacha, Y. Mulgaonkar, C. J. Taylor, and V. Kumar, "Experiments in fast, autonomous, GPS-denied quadrotor flight," in *2018 IEEE International Conference on Robotics and Automation (ICRA)*. IEEE, 2018, pp. 7832–7839.

[19] K. Mohta, M. Watterson, Y. Mulgaonkar, S. Liu, C. Qu, A. Makineni, K. Saulnier, K. Sun, A. Zhu, J. Delmerico *et al.*, "Fast, autonomous flight in GPS-denied and cluttered environments," *Journal of Field Robotics*, vol. 35, no. 1, pp. 101–120, 2018.

[20] S. W. Chen, G. V. Nardari, E. S. Lee, C. Qu, X. Liu, R. A. F. Romero, and V. Kumar, "Sloam: Semantic lidar odometry and mapping for forest inventory," *IEEE Robotics and Automation Letters*, vol. 5, no. 2, pp. 612–619, 2020.

[21] S. Leutenegger, "OKVIS2: Realtime scalable visual-inertial SLAM with loop closure," *arXiv preprint arXiv:2202.09199*, 2022.

[22] D. Tzoumanikas, W. Li, M. Grimm, K. Zhang, M. Kovac, and S. Leutenegger, "Fully autonomous micro air vehicle flight and landing on a moving target using visual–inertial estimation and model-predictive control," *Journal of Field Robotics*, vol. 36, no. 1, pp. 49–77, 2019.

[23] G. Xu, J. Cheng, P. Guo, and X. Yang, "Attention concatenation volume for accurate and efficient stereo matching," in *Proceedings of the IEEE/CVF Conference on Computer Vision and Pattern Recognition*, 2022, pp. 12 981–12 990.

[24] W. Wang, D. Zhu, X. Wang, Y. Hu, Y. Qiu, C. Wang, Y. Hu, A. Kapoor, and S. Scherer, "TartanAir: A dataset to push the limits of visual SLAM," in *2020 IEEE/RSJ International Conference on Intelligent Robots and Systems (IROS)*, 2020.

[25] I. A. Sucan, M. Moll, and L. E. Kavraki, "The open motion planning library," *IEEE Robotics & Automation Magazine*, vol. 19, no. 4, pp. 72–82, 2012.

[26] J. D. Gammell, S. S. Srinivasa, and T. D. Barfoot, "Informed RRT*: Optimal sampling-based path planning focused via direct sampling of an admissible ellipsoidal heuristic," in *IEEE/RSJ International Conference on Intelligent Robots and Systems*, Chicago, IL, USA, September 2014, pp. 2997–3004.

[27] F. L. Markley, Y. Cheng, J. L. Crassidis, and Y. Oshman, "Averaging quaternions," *Journal of Guidance, Control, and Dynamics*, vol. 30, no. 4, pp. 1193–1197, 2007.

[28] Swiss National Forest Inventory, https://lfi.ch/publikationen/publ/LFI_Flyer-en.pdf, 2021.